THE INFLUENCE OF AlFeNiCrCoTi HIGH-ENTROPY ALLOY ON MICROSTRUCTURE, MECHANICAL PROPERTIES AND TRIBOLOGICAL BEHAVIORS OF ALUMINUM MATRIX COMPOSITES

Qinglin Li, Xuepeng Bao, Shang Zhao, Yuqian Zhu, and Yefeng Lan
State Key Laboratory of Advanced Processing and Recycling of Nonferrous Metals, School of Materials Science and Engineering, Lanzhou University of Technology, Lanzhou 730050, China

Xianyu Feng and Qiang Zhang
School of Materials Science and Engineering, Lanzhou University of Technology, Lanzhou 730050, China

Abstract

The microstructure, mechanical properties and tribological behaviors of aluminum matrix composites with different contents of AlFeNiCrCoTi high-entropy alloy (HEA) (4.0, 5.0 and 6.0 wt%) were investigated. The as-cast specimens were analyzed by the scanning electron microscopy and electron probe micro-analysis. The results indicated that flake-like and blocky intermetallic compounds precipitated distributing in α-Al matrix in the solidification when the concentration of HEA was more than 4.0 wt% in pure aluminum. Moreover, as the content of HEA increased, the number of the intermetallic compounds increased. Meanwhile, a new phase formed and it distributed inter-dendrite of α-Al in the solidification, which morphology was rod-shaped and the diameter was less than 200 nm. The area fraction of the nano-phases increased, and the diameter decreased with increasing the addition of HEA in pure aluminum. The tensile test illustrated that the ultimate tensile strength increased firstly and then decreased with the increase of HEA content. When the addition concentration of HEA was 4.0 wt%, the ultimate tensile strength enhanced from 58 to 142 MPa. When 5.0 wt% HEA was added into pure aluminum, the ultimate tensile strength further improved from 142 to 170 MPa. In addition, the elongation decreased from 40.6 to 22.7%. However, when 6.0 wt% HEA was added into pure aluminum, the ultimate tensile strength and elongation reduced to 157 MPa and 18.2%, respectively. The tribological behaviors of aluminum matrix composites were investigated under the condition of seawater. The friction coefficient and wear rate of aluminum matrix composites significantly decreased with the increase of HEA content. Moreover, when the addition level was up to 6.0 wt%, the friction coefficient of aluminum matrix composites decreased by 71.1% from 0.83 to 0.24, and wear rate decreased by 90.8% from $2.48 \times 10^{-9}\ m^3\ N^{-1}\ m^{-1}$ to $2.27 \times 10^{-10}\ m^3\ N^{-1}\ m^{-1}$.

Keywords: aluminum matrix composites, high-entropy alloy, microstructure, mechanical properties, tribological behaviors

Introduction

With the rapid development of science and technology, aluminum matrix composites (AMCs) occupy a crucial position in the aerospace, aircraft and automobile manufacturing industries due to their high wear resistance, high specific strength, light weight, low thermal expansion and stability at elevated temperature. The AMCs are expected to become candidate in the place of casting and wrought aluminum alloys.[1,2] Therefore, researchers made many efforts to investigate the effect of reinforcement on the microstructure, mechanical properties and tribological behavior of AMCs to improve the mechanical properties and wear resistance. There are three types of reinforcements for aluminum and its alloys: particle reinforcement,[3,4] whisker enhancement,[5] and fiber reinforcement.[6] The hardness and deformation resistance of AMCs can significantly improve due to the presence of reinforcement.[7] Yue et al.[8] found that whisker-reinforced AMCs have higher strength, higher hardness and wear resistance than aluminum and its alloys.

In addition, AMCs through carbon fiber-reinforced composites exhibit high strength, high modulus of elasticity and low density.[9,10] Metal matrix composites (MMCs) reinforced with ceramic particles have high specific strength, modulus and excellent high temperature performance.[11–14] The high-entropy alloys (HEAs) are comprised of five or more elements and are different from the traditional multicomponent alloys, which possess high strength, high hardness, wear resistance, good plasticity, oxidation resistance and good physical properties.[15–17] In addition, it has been found that the microstructure of HEAs belongs to a mixture of solid solutions with BCC and FCC and intermetallic compounds.[18,19] Hence, researchers have used high-entropy alloy particles as reinforcing phase to prepare Al-based and Cu-based materials with good comprehensive properties in recent years.[20,21] It has been reported that between the particles of HEA and aluminum matrix have excellent interfacial wettability and compatibility.[20] Hence, the HEA can be used as the reinforcement in order to prepare AMCs. It was reported that $Al_3FeCrCoNi/2024$ composites have been successfully prepared by ball milling, and the compression strength reached 710 MPa under the appropriate hot extrusion process.[22] Karthik et al.[23] fabricated 12 vol% CoCrFeNi/5083 aluminum alloy composites by friction deposition technique and found that the bonding strength was tight on the interface between CoCrFeNi and aluminum matrix, and no intermetallic compounds precipitated from interface. Meanwhile, the yield strength and ductility significantly increased. Chen et al.[21] successfully manufactured copper matrix composites (CMCs) containing 10 wt% and 20 wt% AlCoCrFeNi HEA by powder metallurgical technology. It was found that the HEA did not react with copper atoms on the interface between HEA particles and the copper matrix. After testing the yield strength of the copper matrix and CMCs, it was found that the yield strength of the composites with HEA was enhanced to 240 MPa and 330 MPa, respectively. Luo et al.[24] have successfully prepared 5.0 vol% $Al_{0.25}Cu_{0.75}FeNiCo/7075$ aluminum composites by mechanical alloying method. The elastic modulus enhanced from 71.2 to 79.9 GPa, and the ultimate tensile strength improved from 364.5 to 436.7 MPa. Meanwhile, the elongation also increased from 8.36 to 11.42%. Tan et al.[25] fabricated $Al_{0.6}CoCrFeNi$ HEA by spark plasma sintering (SPS) to reinforce $Al_{65}Cu_{16.5}Ti_{18.5}$ amorphous alloy. The compressive strength of composites was approximately 3120 ± 80 MPa, but the compressive strength of amorphous alloy was only 1700 MPa. However, the method of traditional casting has not been used to prepare the AMCs. The addition of HEA can dissolve into aluminum melt, and then the intermetallic compounds and other phases form, acting as reinforcement in the solidification.

In the previous research, the author found that the addition of trace AlFeNiCrCoTi HEA had a significant effect on the microstructure and mechanical properties of Al–Si alloy. The eutectic silicon was effectively modified, and the strength and elongation enhanced simultaneously. Thus, the author added AlFeNiCrCoTi HEA into pure aluminum melt to fabricate AMCs by traditional casting method. Moreover, the microstructure, mechanical properties and tribological behavior of AMCs were systematically investigated and discussed.

Experiment Procedure

AlFeNiCrCoTi HEA was prepared using high-pure metal of Al, Fe, Ni, Cr, Co and Ti in vacuum arc furnace under the condition of argon protection. The prepared HEA needs to be melted repeatedly 4–5 times in order to ensure the uniformity homogeneous chemical composition.

The commercially available pure aluminum (99.8%) was melted in a Si–C rod heating furnace at 800 °C. Meanwhile, the different amounts of HEA (4.0 wt%, 5.0 wt% and 6.0 wt%) were preheated in the resistance furnace at 800 °C. After the pure aluminum was melted and held for 10 min, the preheated HEA was added into the melt and stirred strongly to ensure the HEA dissolution and guarantee the composition homogenization in aluminum melt. After the melt temperature reduced to 740 °C and degassed with the hexachloroethane (C_2Cl_6), the melt was poured into the steel mold (the diameter 18 mm, the height 140 mm) preheated up to 200 °C. The metallographic specimens were prepared according to the standard metallographic preparation process, and the specimens were corroded with electrolyte ($HClO_3$:C_2H_5OH = 1:9). The microstructural evolution and phases of the specimens were analyzed by field emission scanning electron microscope (SEM) with energy-dispersive X-ray spectroscope (EDS) and electron probe micro-analysis (EPMA). DSC analyzed the exothermic and endothermic peaks in melt and solidification. The tensile specimens were processed into 25 mm in gauge and 5 mm in diameter in terms of the tensile sample standard. The tensile experiment was carried out at a speed of 1 mm/min using universal tensile machine (AG-10TA) by Shimadzu. The average hardness of 5 points was measured by Vickers hardness with a load of 0.2 kg and a dwell time of 10 s. In order to study the wear behavior of AMCs, the 316L steel ball with a diameter of 6 mm was selected as the sliding friction pair. The seawater friction test was conducted by the HSR-2M high-speed reciprocating friction tester with slip rate of 0.15 m/s, load of 10 N and sliding time of 30 min.

Results and Discussion

Microstructure of the Composites

The microstructure of the composites has been analyzed in our literature.[26] Four phases of A12, A2, B2 and D03 exist in AlFeNiCrCoTi HEA, in which A12 and D03 are complex crystal structure and A2 and B2 are simple body-centered cubic (BCC) structure. It has been reported in the
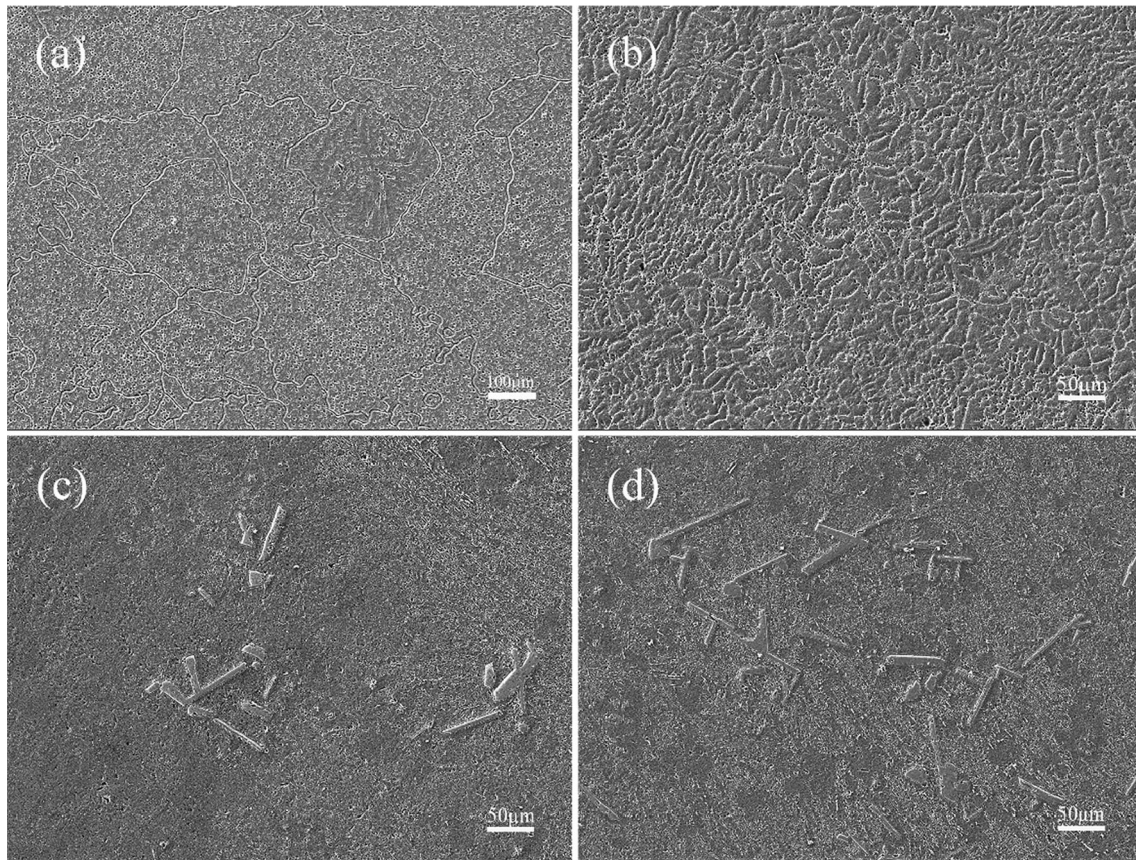
Figure 1. SEM micrographs of aluminum with different addition concentrations of HEA: (a) pure aluminum; (b) 4.0 wt% HEA; (c) 5.0 wt% HEA; (d) 6.0 wt% HEA.

literature that A2 is FeCr-based-type solid solution and B2 is NiAi-based ordered solid solution.[27] The A12 is α-Mn-type solid solution, while D03 is solid solution of AlFe3 type.[28] Figure 1 shows the microstructure of pure aluminum and prepared AMCs with different HEA contents. It can be observed from Figure 1a that the microstructure of pure aluminum is coarse-equiaxed grains and the mean size is about 220 μm. After 4.0 wt% HEA is added to pure aluminum, the size of α-Al grain significantly decreases, and the morphology obviously transforms from coarse
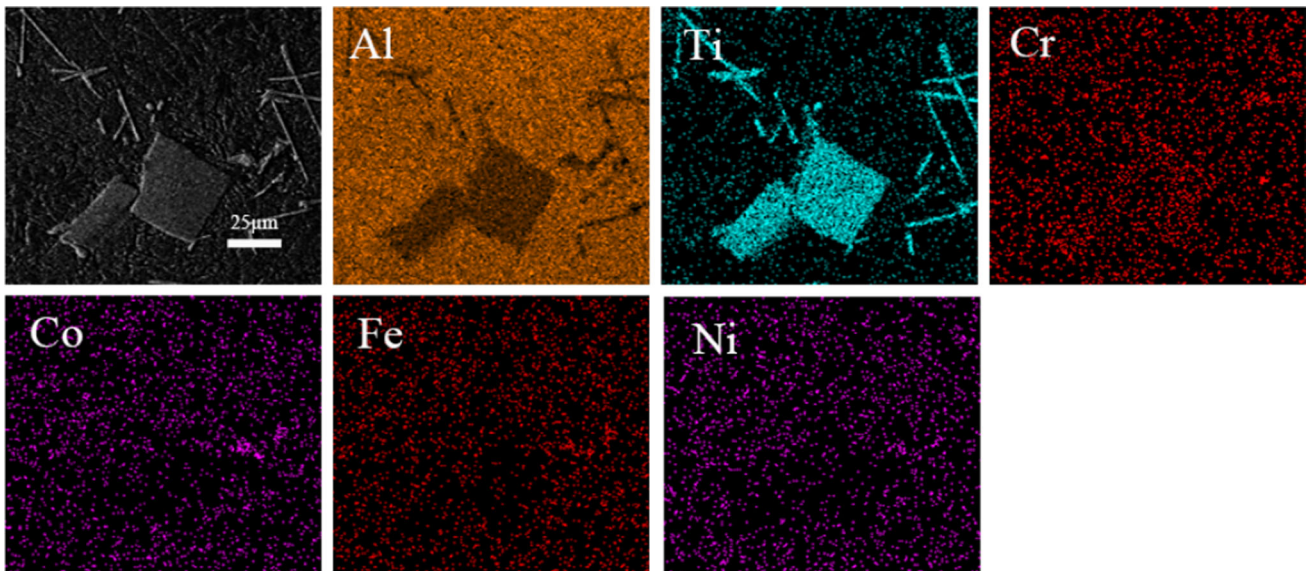
Figure 2. EDS results of aluminum with 6.0 wt% HEA.

equiaxed crystals to dendritic structure due to forming the second phases inter-dendrites of α-Al, as shown in Figure 1b. When the content of HEA increases to 5.0 wt%, it is obvious that intermetallic compounds form distributed in the α-Al matrix in the form of flake and block, as shown in Figure 1c. The average length and width of the flake-like intermetallic compounds are about 53 μm and 8 μm, respectively, whereas the length and width of the blocky intermetallic compounds are about 24 μm. When the content reaches 6.0 wt%, it can be seen from Figure 1d that the morphology of intermetallic is still flake and block, but the number of intermetallic significantly increases and uniformly distributes in matrix. However, the average length and width of the flake-like intermetallic increase to 82 μm and 12 μm, respectively. The sample adding 6.0 wt% HEA to the aluminum melt is analyzed by energy-dispersive X-ray spectroscope (EDS), as shown in Figure 2. The result shows that the flake-like intermetallic is mainly composed of Al and Ti elements. Therefore, the flake-like intermetallic should be Al_3Ti phases. Meanwhile, the blocky intermetallic mainly consists of Al, Ti and Cr elements, whereas Fe, Co and Ni elements uniformly distribute in the α-Al matrix. Therefore, the blocky phases are Al–Ti–Cr ternary intermetallic compounds. Figure 3a, c, e presents the solidified microstructure of AMCs when the different HEA concentrations are added to pure aluminum
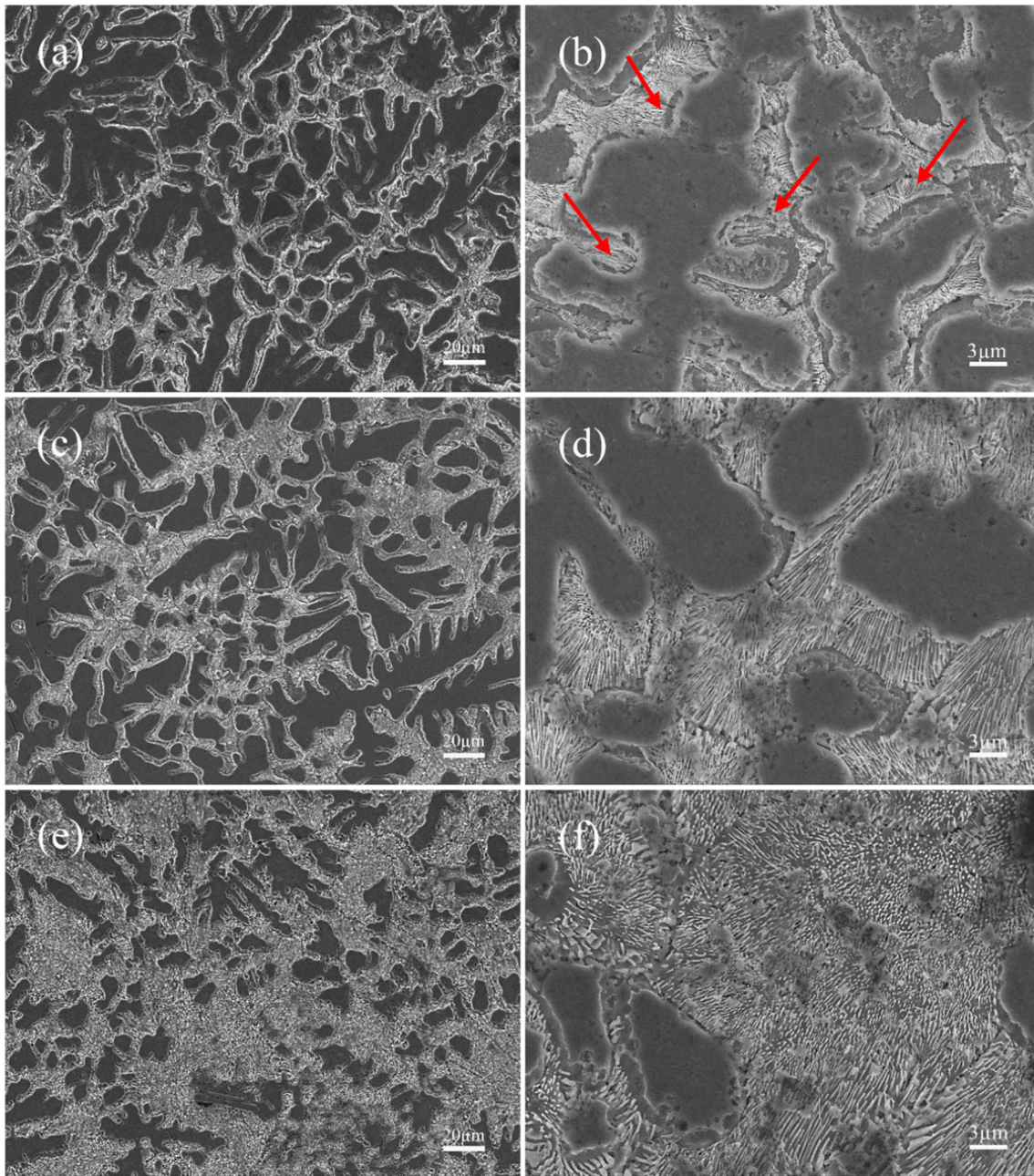

Figure 3. Micrographs of aluminum with different HEA contents: (a) and (b) with 4.0 wt% HEA; (c) and (d) with 5.0 wt% HEA; (e) and (f) with 6.0 wt% HEA.
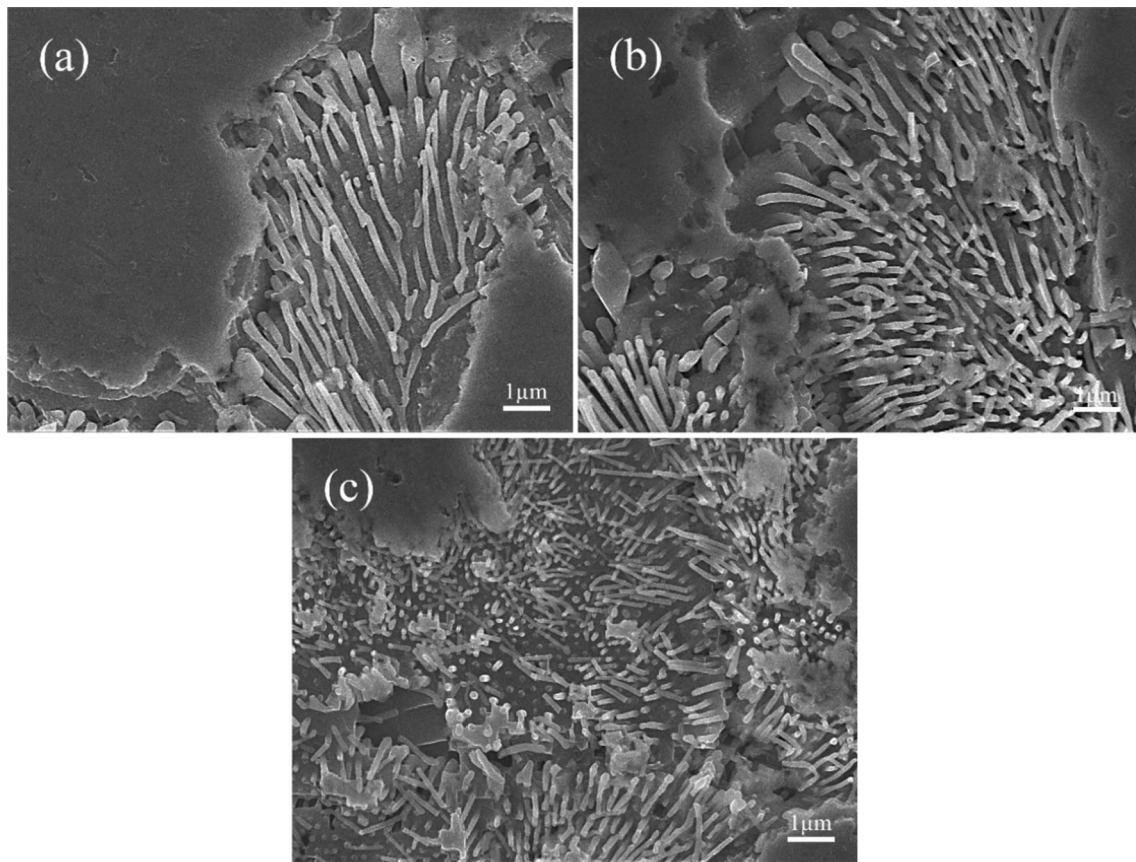
Figure 4. SEM micrographs of new phase in aluminum with different HEA contents: (a) with 4.0 wt% HEA, (b) with 5.0 wt% HEA and (c) with 6.0 wt% HEA.
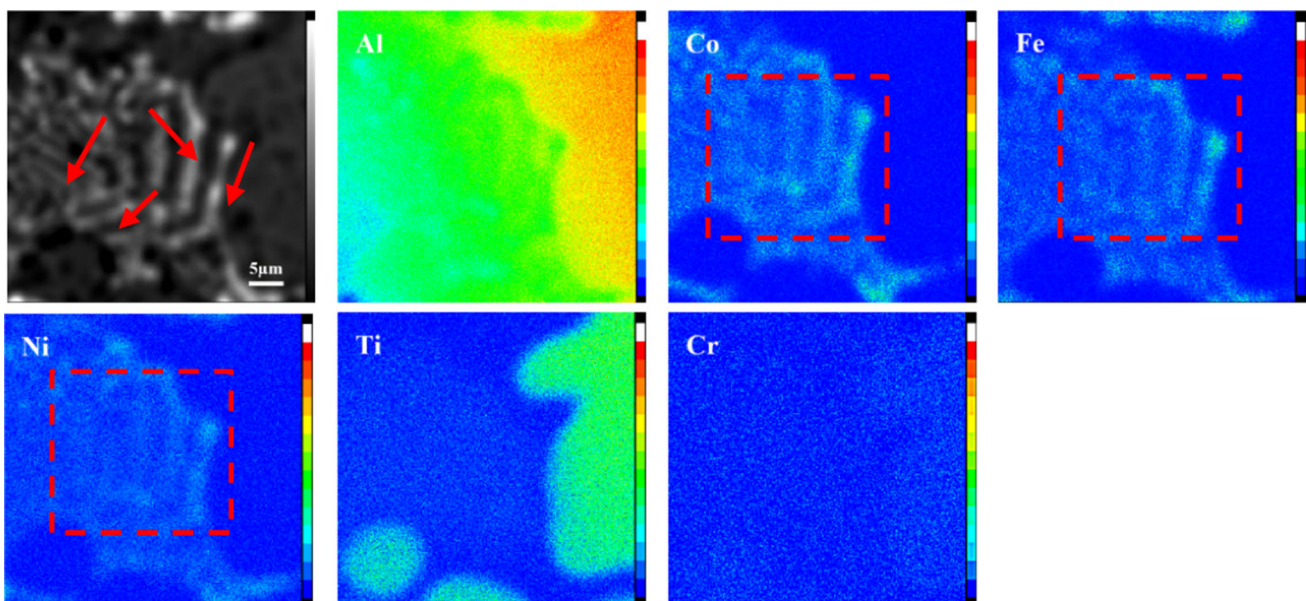

Figure 5. EPMA analysis of aluminum with 6.0 wt% HEA.

melt, whereas Figure 3b, d, f shows magnified image of Figure 3a, c, e, respectively. The solidified microstructure of aluminum adding 4.0 wt% HEA is shown in Figure 3a. It is obviously observed that the α-Al phases exist in the form of dendritic morphology. Moreover, it can be seen

from Figure 3 that the fine second phases form during the solidification and distribute inter-dendrite of α-Al (area indicated by the red arrow). The solidified microstructure of aluminum adding 5.0 wt% HEA is shown in Figure 3c, d. Comparing Figure 3a with c, it can be observed that the

secondary dendrite arm spacing (SDAS) gradually decreases. In addition, the volume fraction of α-Al dendrites also significantly decreases and the volume fraction of fine second phases increases with increasing the addition concentration. When the content of HEA increases to 6.0 wt%, the α-Al dendrites further decrease and the area of fine precipitate distributing inter-dendrite of α-Al increases, as shown in Figure 3e, f.

In order to further analyze the morphology and size of precipitate distributing inter-dendrite of α-Al, the local magnified images are adopted, as shown in Figure 4. When 4.0 wt% HEA is added to pure aluminum melt, it can be seen from the magnified micrograph that the fine second phases in the rod-like morphology exist inter-dendrite of α-Al. Moreover, the diameter of the fine precipitates gradually is reduced from 180 to 157 nm with increasing addition concentration of HEA. After the 6.0 wt% HEA is added into aluminum melt, the diameter of fine phases decreases to 120 nm.

According to the analysis above, the dense second phases should be a nano-sized precipitate, and the growth direction is different in the solidification in different areas. Some nano-phases are perpendicular to the wall of casting mold, but other phases are parallel to the wall of casting mold. Figure 5 shows the typical mapping analysis of the nano-phases of the aluminum with 5.0 wt% HEA. It can be clearly seen that Cr and Ti elements homogeneously distribute in the α-Al matrix besides forming flake-like Al_3Ti and blocky Al–Ti–Cr, but the nano-phases mainly consist of Al, Co, Fe and Ni elements, which shows that the nano-phases distributing inter-dendrite of α-Al should be AlCoFeNi intermetallic compounds. In addition, in order to analyze forming relativity between the α-Al and AlCoFeNi in the solidification, DSC analysis of the specimen adding 3.0 wt% HEA to aluminum melt is performed and the DSC curves of pure aluminum without HEA and with 3.0 wt% HEA are illustrated in Figure 6. It is noted that the aluminum with 3.0 wt% HEA has only one endothermic peak and one exothermic peak, as shown in Figure 6. The result indicates that the nano-phases and α-Al phases simultaneously precipitate in the solidification. Hence, a eutectic reaction occurs in the solidification when HEA dissolves to aluminum melt.

Mechanical Properties

Figure 7 shows the ultimate tensile strength and elongation of AMCs adding different HEA concentrations to the aluminum melt. It can be seen from Figure 7 that the pure aluminum has a very low ultimate tensile strength (only 58 MPa), but the plasticity is very good and the elongation value reaches 40.6%. When the 4.0 wt% HEA is added to pure aluminum melt, the ultimate tensile strength is significantly improved from 58 to 142 MPa. However, the elongation decreases to 26.6%. When the content further increases to 5.0 wt%, the ultimate tensile strength reaches
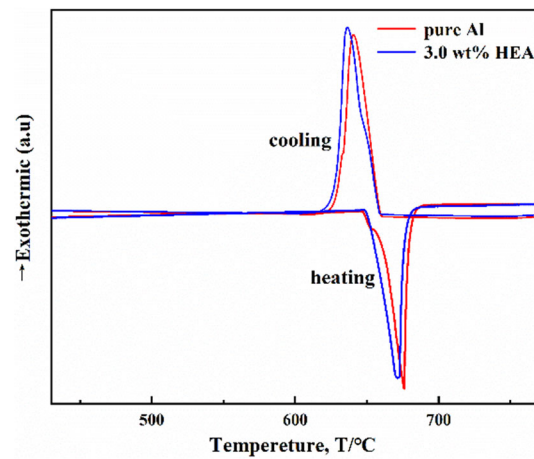

Figure 6. The DSC curve of pure Al without HEA and with HEA.

170 MPa, but the elongation decreases to 22.7%. The microstructural analysis shows that the volume fraction of nano-phase increases and SDAS of α-Al decreases. In addition, flake-like Al_3Ti and blocky Al–Ti–Cr intermetallic compounds precipitate when 5.0 wt% HEA is added into aluminum melt. Moreover, it is worth noticing that some Ti and Cr dissolve to aluminum forming solid solution. Hence, the intermetallic compounds strengthening, solid solution strengthening and grain refinement improve the strength of AMCs. However, when the addition concentration of HEA is up to 6.0 wt%, the ultimate tensile strength and elongation decrease to 157 MPa and 18.2%, respectively. On the one hand, this may be because of the increase of flake-like Al_3Ti and blocky Ai–Ti–Cr intermetallic compounds with the hard and brittle properties leading to the local stress concentration. On the other hand, the interfacial bonding strength is weakened between the intermetallic compounds and the matrix. The result is agreement with the previous literature.[29]

Figure 8 shows the SEM images of fracture surface. It is illustrated that the fracture surface of pure aluminum is
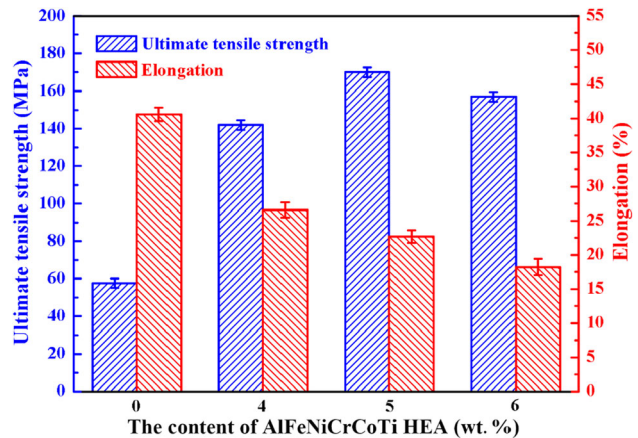

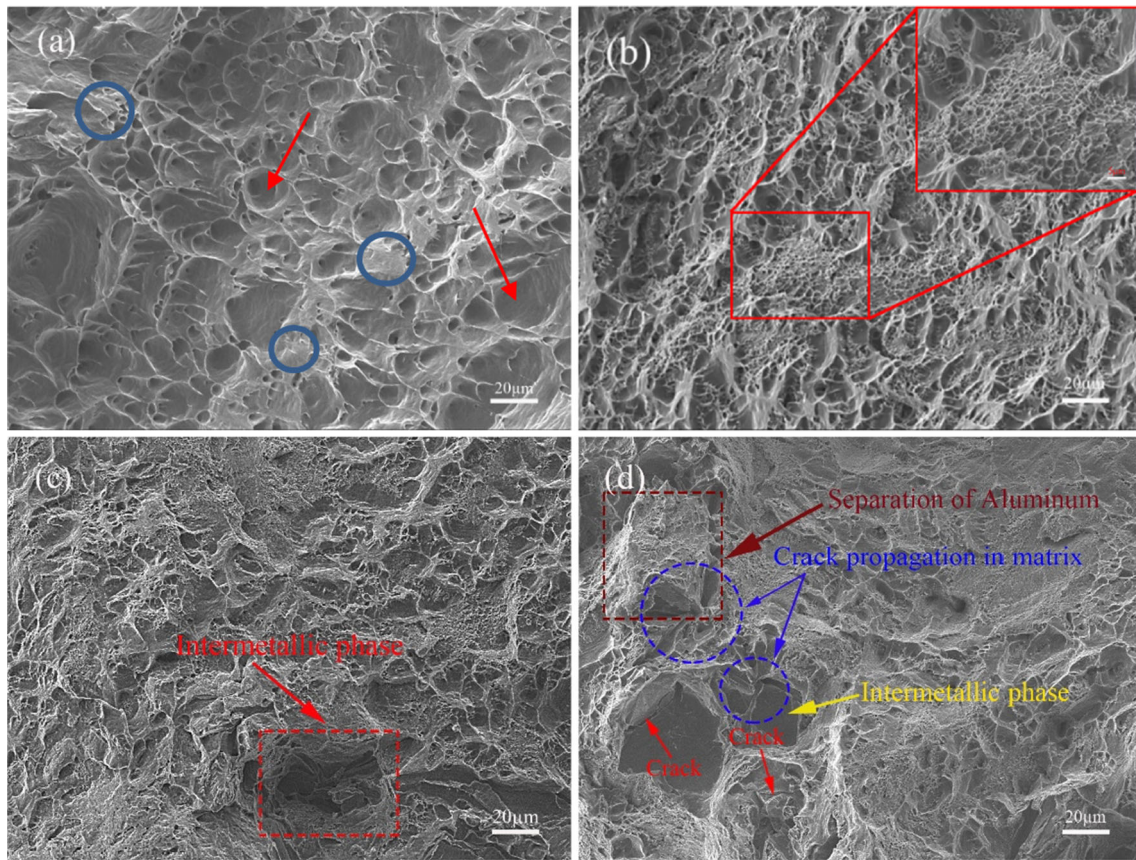**Figure 7. Mechanical properties of aluminum with various HEA concentrations.**

Figure 8. SEM image of fracture surface of aluminum with various HEA concentrations: (a) pure aluminum; (b) 4.0 wt% HEA; (c) 5.0 wt% HEA; (d) 6.0 wt% HEA.
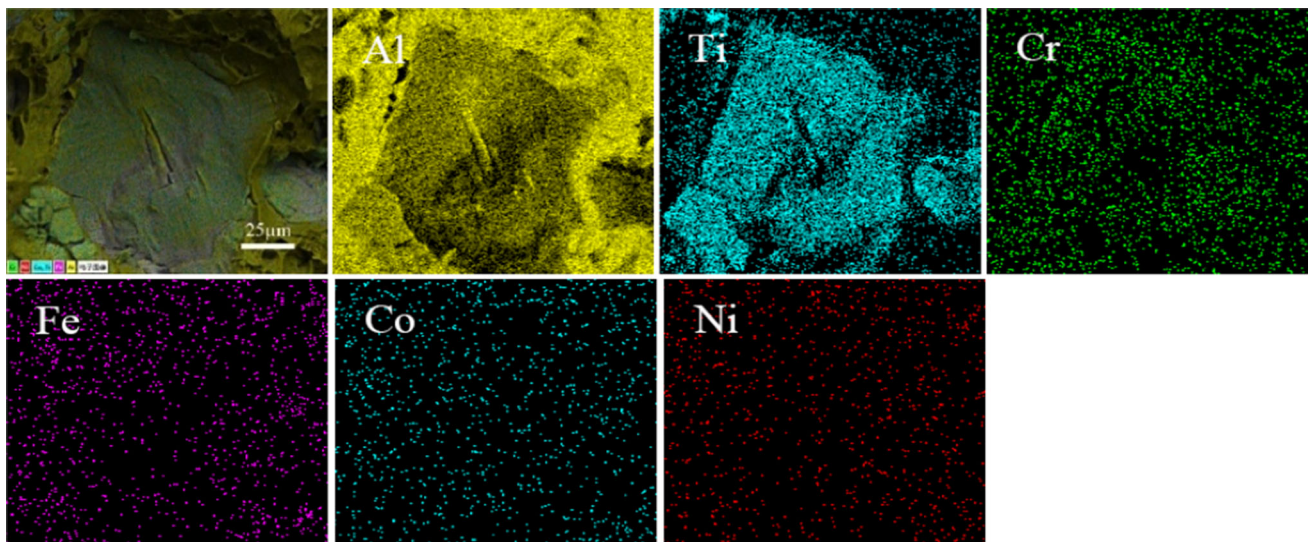

Figure 9. EDS results on fracture surface of aluminum with 6.0 wt% HEA.

covered by many uniform dimples, as shown in Figure 8a. Figure 8b shows fracture surface of aluminum with the addition concentration of 4.0 wt% HEA. It can be clearly found that the dimple size reduces compared with pure aluminum. As the content of HEA increases to 5.0 wt%, the cleavage plane appears on the fracture surface (marked by red square), and the number of dimples significantly reduces, as shown in Figure 8c. When the addition of HEA reaches 6.0 wt%, the blocky intermetallic compounds appears on the fracture surface (marked by yellow arrow), and cracks generate at the tip of the intermetallic compound due to large stress concentration (marked by red
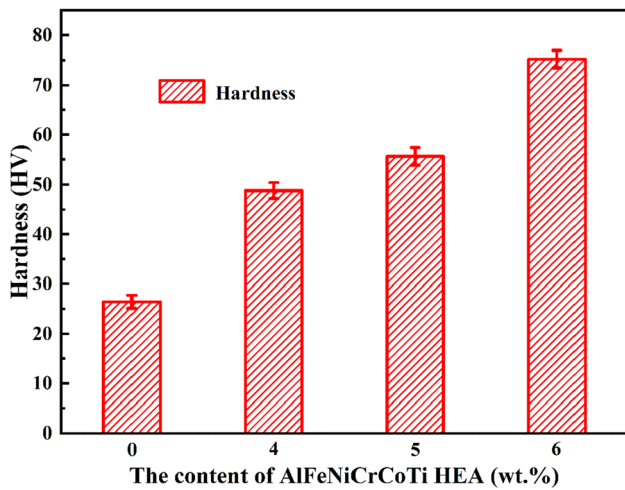
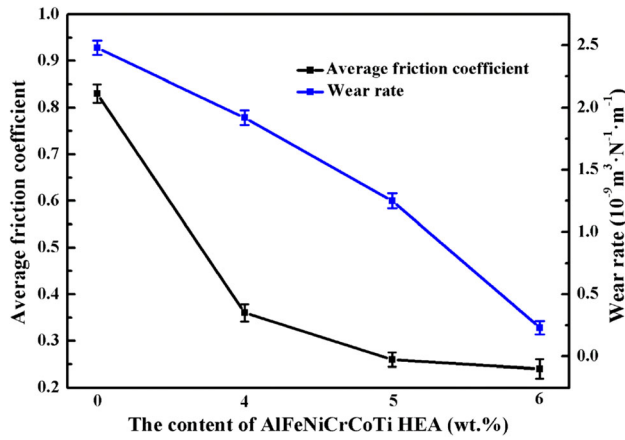**Figure 10. Hardness of aluminum with various HEA contents.**

Figure 11. Average friction coefficient and wear rate of aluminum with various HEA contents.

arrow). Figure 9 shows SEM–EDS images of fracture surface of the sample, which is prepared by adding 6.0 wt% HEA to the aluminum melt. According to the mapping analysis, it can be inferred that the blocky phase is Al–Ti–Cr intermetallic compounds with hard and brittle properties. In addition, the blocky Al–Ti–Cr compounds present sharp edges or ends leading to stress concentration, where the cracks more easily form than that of matrix in tensile tests. The cracks primarily initiate and propagate along the interfaces between intermetallic and aluminum matrix, and then the neighboring cracks link and cause the fracture of the materials. Therefore, the ultimate tensile strength decreases with increasing addition concentration of HEA.

Hard and Friction Properties

Figure 10 shows the hardness values of pure aluminum and AMCs. It can be clearly seen that the hardness of pure aluminum is only 26.4 HV, but the hardness value of the composites is significantly improved with increasing

addition concentration of HEA. When 4.0 wt% HEA is added to pure aluminum, the hardness of the AMCs is 48.8 HV. When 5.0 wt% HEA is introduced into pure aluminum, the hardness value increases to 55.6 HV. When the content reaches 6.0 wt%, the hardness value of the preparing AMCs increased by 184.8% from 26.4 to 75.2 HV. This is because the formation of hard Al_3Ti and Al–Ti–Cr intermetallic compounds exists in the matrix.

The average friction coefficient and wear rate of aluminum with different addition concentrations of HEA preparing AMCs were measured in order to characterize the tribological behaviors of AMCs under the seawater environment, as shown in Figure 11. The friction coefficient and wear rate of pure aluminum are 0.83 and 2.48×10^{-9} m^3 N^{-1} m^{-1}, respectively. After the addition of HEA, the friction coefficient and wear rate of AMCs are significantly decreased. When 4.0 wt% HEA is added to pure aluminum, the friction coefficient and wear rate of AMCs decrease to 0.36 and 1.92×10^{-9} m^3 N^{-1} m^{-1}, respectively. Further increasing the addition level of HEA to 5.0 wt% and 6.0 wt%, the friction coefficient rate of AMCs is 0.26 and 0.24, and the wear rate is 1.25×10^{-9} m^3 N^{-1} m^{-1} and 2.27×10^{-10} m^3 N^{-1} m^{-1}, respectively. The friction coefficient and wear rate of AMCs are smaller than that of pure aluminum. This is because pure aluminum has low strength, low hardness and low plastic deformation resistance. Hence, it is easy to form a solder joint on the contact surface during the sliding friction process. In addition, the presence of hard Al_3Ti and Al–Ti–Cr phases in the matrix leads to increasing hardness and wear resistance of AMCs.

Figure 12 demonstrates the SEM images of worn surface of AMCs adding various HEA concentrations. Figure 12a shows the friction surface of pure aluminum. Due to low hardness of pure aluminum, there are a few of obvious scratches and furrows on the surface. The friction surface is cracked into pieces forming on the surface due to the large plastic deformation during sliding friction. Figure 12b–d indicates the friction morphology of preparing different AMCs. It can be seen that there are significant craters and grooves on the friction surface denoted by yellow arrows in Figure 12b. However, as the HEA content increases, the craters and grooves become narrower denoted by yellow arrows in Figure 12c, d. According to the analysis above, the wear mechanism of pure aluminum is mainly adhesive wear, but the wear mechanism of AMCs is abrasive wear. Worn surface of pure aluminum is analyzed by EDS, as shown in Figure 13. It is proved that the friction surface mainly contains Al and O on the surface. The result shows that the wear surface is oxidized during the friction. In addition, worn surface of aluminum with 6.0 wt% HEA addition is also analyzed by EDS, as shown in Figure 14. The friction surface of AMCs is mainly composed of Al, Ti and Cr, which shows the formation of Al–Ti-Cr intermetallic compounds improving wear resistance. Comparing Figures 13 with 14, it is easy to find that the oxygen
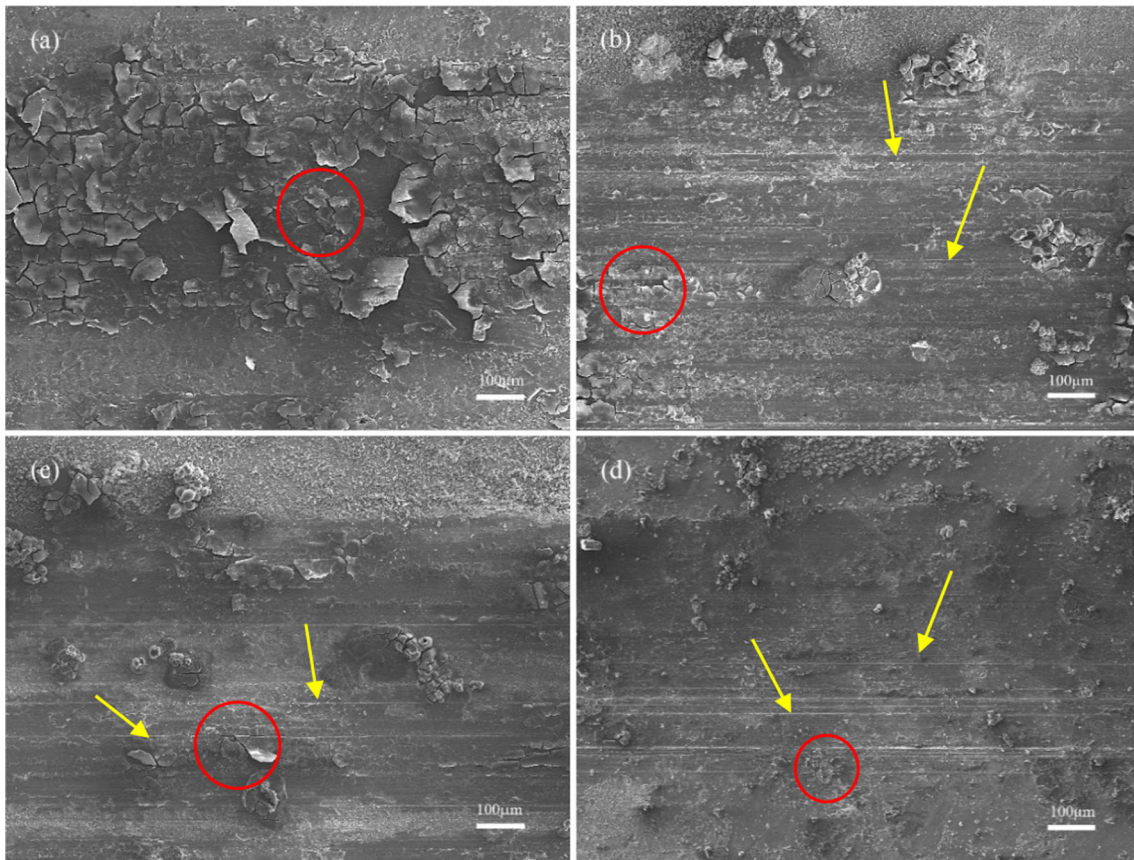
Figure 12. The worn surfaces of aluminum with different HEA contents: (a) pure aluminum; (b) 4.0 wt% HEA; (c) 5.0 wt% HEA; (d) 6.0 wt% HEA.
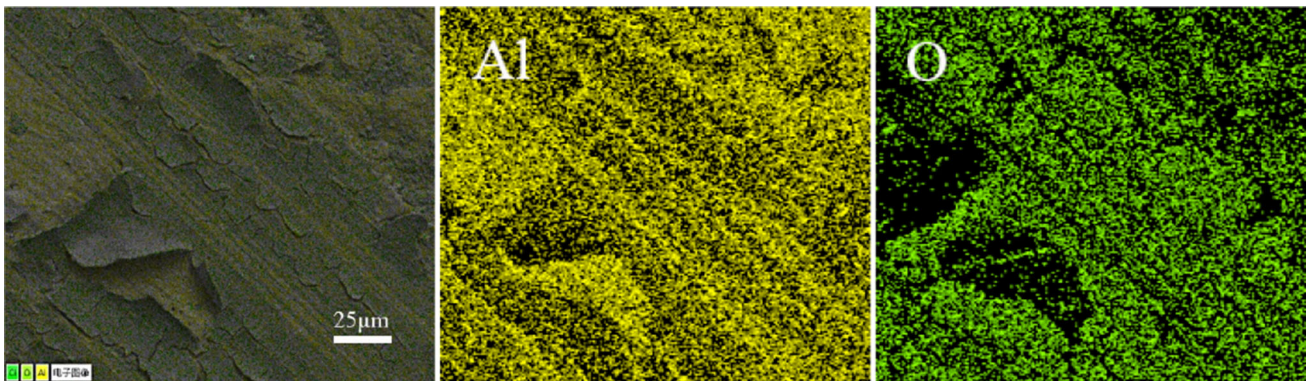

Figure 13. EDS results on worn surface of pure aluminum.

content in the wear surface of the pure aluminum is higher than that of AMCs. The addition of HEA improves the oxidation resistance of AMCs. In addition, it can be observed that the friction surface of pure aluminum and AMCs has cracking phenomenon (marked by red circle) due to the normal stress and fatigue during the sliding process,[30] and the cracking phenomenon is weakened with increasing HEA content, as shown in Figure 12a–d. This is because the brittle oxides are easily formed on the surface of the pure aluminum during the friction process, and these brittle oxides largely fall off from the surface during friction and wear.[31] In addition, the friction surface of AMCs forms fine wear particles due to the presence of Al_3Ti and Al–Ti-Cr hard phase during the sliding friction process.[32]
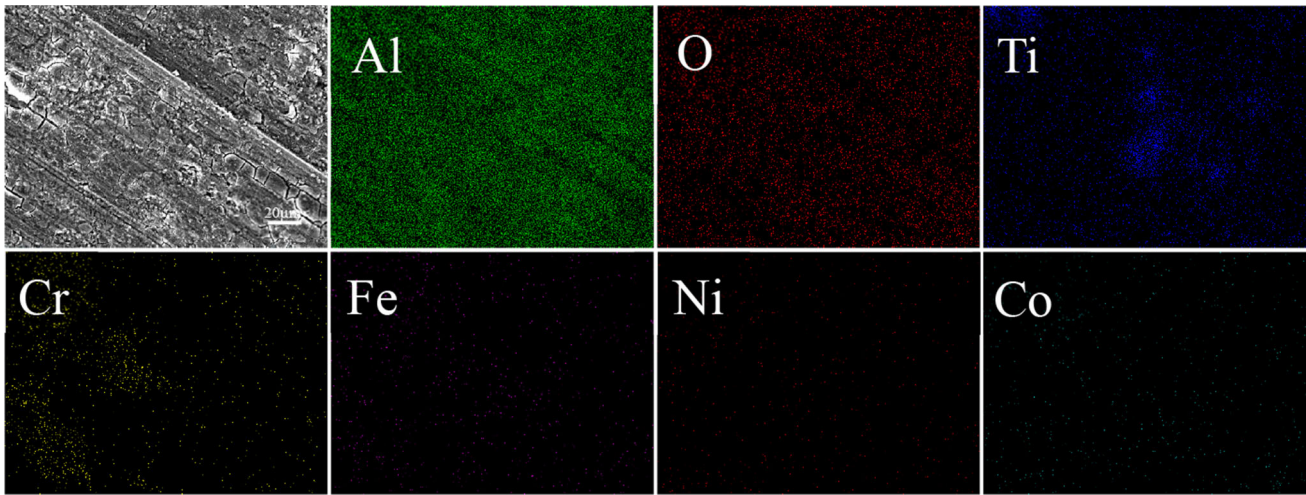
Figure 14. EDS results on worn surface of aluminum with 6.0 wt% HEA.

Conclusions

The effects of HEA concentration on the microstructure, mechanical properties and the tribological behavior of aluminum were studied. Through the analysis, the conclusions can be summarized:

(1) When HEA is added to pure aluminum melt, α-Al dendrites are significantly refined. The flake-like Al₃Ti and blocky Al–Ti–Cr intermetallic compounds precipitate, and the dense nano-phases of Al–Co–Fe–Ni form, which exist in the form of rod-shaped morphology.

(2) The ultimate tensile strength increased by 193.1% from 58 to 170 MPa with the increase of the addition level of HEA. However, the elongation decreased by 44.1% from 40.6 to 22.7%.

(3) The hardness value improved by 184.8% from 26.4 to 75.2 HV after the addition of 6.0 wt% HEA.

(4) The friction coefficient is decreased by 71.1% from 0.83 to 0.24 and wear rate reduced by 90.8% from 2.48×10^{-9} m^3 N^{-1} m^{-1} to 2.27×10^{-10} m^3 N^{-1} m^{-1} when the addition of HEA is 6.0 wt%.

Acknowledgements

REFERENCES

1. X. Kai, K. Tian, C. Wang, L. Jiao, G. Chen, Y. Zhao, Effects of ultrasonic vibration on the microstructure and tensile properties of the nano ZrB₂/2024Al composites synthesized by direct melt reaction. J. Alloys Compd. **668**, 121–127 (2016)

2. Y. Tang, Z. Chen, A. Borbely, G. Ji, S.Y. Zhong, D. Schryvers, V. Ji, H.W. Wang, Quantitative study of particle size distribution in an in situ grown Al–TiB₂ composite by synchrotron X-ray diffraction and electron microscopy. Mater. Charact. **102**, 131–136 (2015)

3. Y. Yang, S.F. Wen, Q.S. Wei, W. Li, J. Liu, Y.S. Shi, Effect of scanline spacing on texture, phase and nano hardness of TiAl/TiB₂ metal matrix composites fabricated by selective laser melting. J. Alloys Compd. **728**, 803–814 (2017)

4. F. Ali, S. Scudino, M.S. Anwar, R.N. Shahid, V.C. Srivastava, V. Uhlenwinkel, M. Stoica, G. Vaughan, J. Eckert, Al-based metal matrix composites reinforced with Al–Cu–Fe quasi crystalline particles: strengthening by interfacial reaction. J. Alloys Compd. **607**, 274–279 (2014)

5. C.X. Zhang, D.X. Yao, J.W. Yin, K.H. Zuo, Y.F. Xia, H.Q. Liang, Effects of β-Si₃N₄ whiskers addition on mechanical properties and tribological behaviors of Al matrix composites. Wear **430–431**, 145–156 (2019)

6. J.J. Zhang, S.C. Liu, Y.P. Lu, Y. Dong, T.J. Li, Fabrication process and bending properties of carbon fibers reinforced Al-alloy matrix composites. J. Mater. Process. Technol. **231**, 366–373 (2016)

7. S.C. Tjong, Novel nanoparticle-reinforced metal matrix composites with enhanced mechanical properties. Adv. Eng. Mater. **9**, 639–652 (2007)

8. H.Y. Yue, S.S. Song, B. Wang, X. Gao, L. Yao, S.L. Zhang, L.H. Yao, X.Y. Lin, E.H. Guan, H.J. Zhang, E.J. Guo, Effects of whisker surface treatment on microstructures, tensile properties and aging behaviors

of $Al_{18}B_4O_{33}w$/6061Al composites. J. Alloys Compd. **697**, 11–18 (2017)

9. D.B. Miracle, Metal matrix composites—from science to technological significance. Compos. Sci. Technol. **65**, 2526–2540 (2005)

10. S. Chand, Carbon fibers for composites. J. Mater. Sci. **35**, 1303–1313 (2000)

11. C.R. Si, X.L. Tang, X.J. Zhang, J.B. Wang, W. Wu, Microstructure and mechanical properties of particle reinforced metal matrix composites prepared by gas–solid two-phase atomization and deposition technology. Mater. Lett. **201**, 78–81 (2017)

12. S.F. Li, K. Kondoh, H. Imai, B. Chen, L. Jia, J. Umeda, Y. Fu, Strengthening behavior of in situ-synthesized (TiC–TiB)/Ti composites by powder metallurgy and hot extrusion. Mater. Des. **95**, 127–132 (2016)

13. D.R. Ni, L. Geng, J. Zhang, Z.Z. Zheng, Effect of B_4C particle size on microstructure of in situ titanium matrix composites prepared by reactive processing of Ti–B_4C system. Scr. Mater. **55**, 429–432 (2006)

14. X.L. Guo, Q. Guo, J.H. Nie, Z.Y. Liu, Z.Q. Li, G.L. Fan, D.B. Xiong, Y.S. Su, J.Z. Fan, D. Zhang, Particle size effect on the interfacial properties of SiC particle-reinforced Al–Cu–Mg composites. Mater. Sci. Eng. A **711**, 643–649 (2018)

15. J.W. Yeh, S.K. Chen, S.J. Lin, J.Y. Gan, T.S. Chin, T.T. Shun, Nanostructured high entropy alloys with multiple principal elements: novel alloy design concepts and outcomes. Adv. Eng. Mater. **6**, 299–303 (2004)

16. W.P. Chen, Z.Q. Fu, S.C. Fang, H.Q. Xiao, D.Z. Zhu, Alloying behavior, microstructure and mechanical properties in a $FeNiCrCo_{0.3}Al_{0.7}$ high entropy alloy. Mater. Des. **51**, 854–860 (2013)

17. X. Chen, J.Q. Qi, Y.W. Sui, Y.Z. He, F.X. Wei, Q.K. Meng, Z. Sun, Effects of aluminum on microstructure and compressive properties of Al–Cr–Fe–Ni eutectic multi-component alloys. Mater. Sci. Eng. A **681**, 25–31 (2017)

18. B.S. Murty, J.W. Yeh, S. Ranganathan, *High-Entropy Alloys* (Elsevier, Amsterdam, 2014)

19. Y. Zhang, T.T. Zuo, Z. Tang, M.C. Gao, K.A. Dahmen, P.K. Liaw, Z.P. Lu, Microstructures and properties of high-entropy alloys. Prog. Mater. Sci. **61**, 1–93 (2014)

20. Z.W. Yuan, W.B. Tian, F.G. Li, Q.Q. Fu, Y.B. Hu, X.G. Wang, Microstructure and properties of high-entropy alloy reinforced aluminum matrix composites by spark plasma sintering. J. Alloys Compd. **806**, 901–908 (2019)

21. J. Chen, P.Y. Niu, T. Wei, L. Hao, Y.Z. Liu, X.H. Wang, Y.L. Peng, Fabrication and mechanical properties of AlCoNiCrFe high-entropy alloy particle reinforced Cu matrix composites. J. Alloys Compd. **649**, 630–634 (2015)

22. Z.W. Wang, Y.B. Yuan, R.X. Zheng, K. Ameyama, C.L. Ma, Microstructures and mechanical properties extruded 2024 aluminum alloy reinforced by $FeNiCrCoAl_3$ particles. Trans. Nonferrous Met. Soc. China **24**(2014), 2366–2373 (2024)

23. G.M. Karthik, S. Panikar, G.D. Janaki Ram, R.S. Kottada, Additive manufacturing of an aluminum matrix composite reinforced with nanocrystalline high-entropy alloy particles. Mater. Sci. Eng. A **679**, 193–203 (2016)

24. M.Q. Luo, D.Z. Zhu, L.F. Qi, Q. Chen, L.J. Li, Properties of $Al_xCuFeNiCo$ (Cr) high entropy alloys particles reinforced aluminum alloy materials. South. Met. **6**, 18–22 (2016)

25. Z. Tan, L. Wang, Y.F. Xue, P. Zhang, T.Q. Cao, X.W. Cheng, High-entropy alloy particle reinforced Al-based amorphous alloy composite with ultrahigh strength prepared by spark plasma sintering. Mater. Des. **109**, 219–226 (2016)

26. Q.L. Li, S. Zhao, B.Q. Li, A novel modifier on the microstructure and mechanical properties of Al–7Si alloys. Mater. Lett. **251**, 156–160 (2019)

27. S. Singh, N. Wanderka, B.S. Murty, U. Glatzel, J. Banhart, Decomposition in multi-component AlCoCrCuFeNi high-entropy alloy. Acta Mater. **59**, 182–190 (2011)

28. V. Soare, D. Mitrica, I. Constantin, V. Badilita, F. Stoiciu, A.-M.J. Popescu, I. Carcea, Influence of remelting on microstructure, hardness and corrosion behaviour of AlCoCrFeNiTi high entropy alloy. Mater. Mater. Sci. Technol. **31**, 1194–1200 (2015)

29. K. Abedi, M. Emamy, The effect of Fe, Mn and Sr on the microstructure and tensile properties of A356–10% SiC composite. Mater. Sci. Eng. A **527**, 3733–3740 (2010)

30. S. Taktak, M.S. Baspinar, Observation of delamination wear of lubricious tribo-film formed on Si_3N_4 during sliding against WC-Co in humidity air. Tribol. Int. **39**, 39–49 (2006)

31. N. Akaberi, R. Taghiabadi, A. Razaghian, Effect of bifilm oxides on the dry sliding wear behavior of Fe-rich Al–Si alloys. J. Tribol. **139**, 1254–1263 (2017)

32. A.N. Anasyida, A.R. Daud, M.J. Ghbyajali, Dry sliding wear behavior of Al–4Si–4Mg alloys by the addition of cerium. Int. J. Mech. Mater. Eng. **4**, 127–130 (2009)